

Radiation design in computed tomography via convex optimization

Anatoli Juditsky ^{*} Arkadi Nemirovski [†]

Michael Zibulevsky[‡]

January 13, 2023

Abstract

Proper X-ray radiation design (via dynamic fluence field modulation, FFM) allows to reduce effective radiation dose in computed tomography without compromising image quality. It takes into account patient anatomy, radiation sensitivity of different organs and tissues, and location of regions of interest. We account all these factors within a general convex optimization framework.

1 Introduction

Recently, there has been significant research interest in dynamic fluence field modulation (FFM), which consists in varying the beam shape throughout the scan allowing for the adaptation of the spatial x-ray distribution to conform to the patient anatomy (cf., e.g., [1] and references therein). A range of hardware solutions have been proposed, including dynamic wedges [2, 3, 4], fluid-filled chambers [5, 6, 7, 8], and slitbased multiple aperture devices [9, 10].

Until now, to the best of our knowledge, the problem of FFM radiation planning has been treated within non-convex optimization framework, and only rough distribution of radiation with relatively small number of parameters (coefficients of basis functions) was modeled. In this work we utilize convex optimization techniques to optimize the fine structure of the fluence, namely, the amount of radiation sent into each projection bin (towards the corresponding detector pixel).

^{*}LJK, Université Grenoble Alpes, 700 Avenue Centrale, 38401 Domaine Universitaire de Saint-Martin-d'Hères, France anatoli.juditsky@univ-grenoble-alpes.fr

[†]Georgia Institute of Technology, Atlanta, Georgia 30332, USA, nemirovs@isye.gatech.edu

[‡]Department of Computer Science, Technion—Israel Institute of Technology, Haifa 32000, Israel, mzib@cs.technion.ac.il

This work was supported by Multidisciplinary Institute in Artificial intelligence MIAI @ Grenoble Alpes (ANR-19-P3IA-0003) and by the Israel Council For Higher Education—Planning & Budgeting Committee

The main body of this paper is organized as follows. In Section 2 we present the CT observation model underlying our derivations, introduce and motivate the *loss index* of radiation design responsible for the asymptotical, as the total amount of radiation grows, quality of the Maximum Likelihood recovery of the image of interest. We then pose the problem of optimal radiation design as the problem of optimizing the loss index under general convex constraints on the design. The resulting optimization problem is convex and thus efficiently solvable (at least in theory, and to some extent, also in practice). In Section 3, we report on the (in our appreciation, encouraging) results of a “proof of concept” numerical experiment implementing the radiation design proposed in Section 2. Section 4 contains some concluding remarks.

2 CT Radiation Design

2.1 CT observation scheme

The CT observation scheme we intend to consider is as follows:

1. $x \in \mathbf{R}_+^n$ is the “signal” – the discretized body attenuation density, so that n is the number of voxels in the field of view;
2. $w \in \mathbf{R}^m$ is the vector of observations; observations are indexed by bins, m being the total number of bins;
3. $A \in \mathbf{R}^{m \times n}$ is the “projection matrix”;
4. $q \in \mathbf{R}_+^n$ is the vector with entries q_i which are the expected numbers of photons sent to bin i during the study.

We assume that the i -th observation stemming from signal x is

$$\omega_i \sim \text{Poisson}(q_i \exp\{-[Ax]_i\}), \quad (1)$$

where $\text{Poisson}(\mu)$ is the Poisson distribution with parameter $\mu \geq 0$:

$$\text{Prob}_{\iota \sim \text{Poisson}(\mu)}\{\iota = k\} = \frac{\mu^k}{k!} e^{-\mu}, \quad k = 1, 2, \dots$$

We assume also that entries ω_i in the vector of observations ω are independent across $i = 1, \dots, m$.

5. Given observation ω stemming from the unknown signal x , we want to recover the vector Bx , where $B \in \mathbf{R}^{\nu \times n}$ is a given matrix.¹ We measure the recovery error in the standard Euclidean norm $\|\cdot\|_2$ on \mathbf{R}^ν .

¹In our experiments Bx is a truncation of image x towards the region of interest (ROI).

2.2 Radiation sensitivity - from voxels to bins

Informally, our goal is to find radiation design q , which provides best image quality given the whole-body effective dose. Various organs and tissues have different sensitivity to radiation—effective dose caused by unitary radiation exposure. This can be reflected in 3D voxel-wise sensitivity map s , which is standardly used in radiation therapy planning.

We assume that, in addition, an (approximate) attenuation map of the body is available, and we can compute an auxiliary bin-sensitivity vector c with entries c_i reflecting effective dose obtained from a unit of radiation sent into bin i . Constant whole body effective dose is provided by the condition

$$c^T q = \text{const}, \quad (2)$$

Thus our goal is to find radiation design q , which provides the best image quality under constraint (2).

2.3 Maximum Likelihood estimate

With A and q given, we intend to recover Bx as $B\hat{x}(\omega)$, where $\hat{x}(\omega)$ is the Maximum Likelihood (ML) estimate. Denoting by a_i^T , $i = 1, 2, \dots, m$, the rows of A , the log-likelihood of observing ω , the signal being x , is

$$\begin{aligned} \mathcal{L}_q(\omega, x) &= \sum_{i=1}^m [\omega_i \ln(q_i \exp\{-a_i^T x\}) - q_i \exp\{-a_i^T x\} - \ln(\omega_i!)] \\ &= \sum_{i=1}^m [-\omega_i a_i^T x - q_i \exp\{-a_i^T x\}] + R(q, \omega). \end{aligned}$$

Consequently, maximizing $\mathcal{L}_q(\omega, x)$ in x is the same as maximizing in x the concave in x function

$$L_q(x) - [\sum_i \omega_i a_i]^T x, \quad L_q(x) = -\sum_i q_i \exp\{-a_i^T x\} \quad (3)$$

and is therefore an efficiently solvable problem; the resulting estimate

$$\hat{x}(\omega) \in \underset{x}{\text{Argmax}} \left[L_q(x) - [\sum_i \omega_i a_i]^T x \right]$$

of x is a function of ω depending on q as a parameter.

2.4 Radiation Design via Loss index minimization

Our goal is “presumably good,” in terms of the performance of the resulting estimate, selection of q in a given compact convex set $\mathcal{Q} \subset \mathbf{R}_+^m$. This informal goal can be stated formally in different ways; the formalization we propose is based on the following observation.

A. In the “noiseless case” where the observations are $\omega_i = \mu_i$, $\mu_i = q_i \exp\{-a_i^T x_*\}$, x_* being the true signal (instead of being Poisson random variables with parameters μ_i), the ML estimate exactly recovers the true signal. In other words,

setting $\gamma_* = \sum_i \mu_i a_i$, we get $x_+ \in \text{Argmax}_x [L_q(x) - \gamma_*^T x]$. Indeed, since L_q is concave and smooth in x , it suffices to verify that $\nabla_x L_q(x_*) = \gamma_*$, which is evident.

B. Now assume that the positive semidefinite Hessian matrix

$$H := -\nabla^2 L_q(x_*) = \sum_i \mu_i a_i a_i^T$$

is positive definite, or, which is the same when $q > 0$, that A is of rank m . Let $\bar{L}_q(\cdot)$ be the second order Taylor approximation of $L_q(\cdot)$ around $x = x_*$. Were we specifying our estimate of x as

$$\tilde{x} = \tilde{x}(\omega) := \underset{x}{\text{argmax}} [\bar{L}_q(x) - [\sum_i \omega_i a_i]^T x],$$

we would have

$$\nabla_x \bar{L}_q(\tilde{x}) = \sum_i \omega_i a_i, \quad \nabla_x \bar{L}(x_*) = \sum_i \mu_i a_i,$$

that is, $\tilde{x} - x_* = -H^{-1} \underbrace{\sum_i [\omega_i - \mu_i] a_i}_{\delta}$. Hence, taking into account the immediate

relation $\mathbf{E}\{\delta \delta^T\} = H$ (recall that $\omega_i \sim \text{Poisson}(\mu_i)$ are independent across i),

$$\begin{aligned} \mathbf{E}\{\|B\tilde{x} - Bx_*\|_2^2\} &= \mathbf{E}\{\delta^T H^{-1} B^T B H^{-1} \delta\} = \mathbf{E}\{\text{Tr}(H^{-1} B^T B H^{-1} \delta \delta^T)\} \\ &= \text{Tr}(H^{-1} B^T B H^{-1} \mathbf{E}\{\delta \delta^T\}) = \text{Tr}(H^{-1} B^T B) \\ &= \text{Tr}(B H^{-1} B^T). \end{aligned}$$

This computation suggests, as a meaningful ‘‘loss index’’ of q (the smaller it is, the better for our purposes) the function

$$\mathcal{I}_*(q) = \text{Tr} \left(B \left[\sum_i q_i \exp\{-a_i^T x_*\} a_i a_i^T \right]^{-1} B^T \right) \quad (4)$$

Needless to recall, the above reasoning is informal—our estimate of x is not \tilde{x} , it is \hat{x} . Nevertheless, it can be proved that when A is of rank m and q becomes large, specifically, $q = t\bar{q}$ with $\bar{q} > 0$, when $t \rightarrow \infty$, our informal reasoning yields correct asymptotics of the expected squared $\|\cdot\|_2$ -error of the recovery of Bx^2 . We, however, neither present these asymptotic results, nor need them—our goal at this point is to find a convenient criterion to be optimized over $q \in \mathcal{Q}$ in order to get a presumably good measurement design, and to this end no rigorous justification of our choice is needed. What indeed is important for us, is that \mathcal{I}_* is a convex function of $q > 0$, and thus is well suited for minimization.

A bad news is that strictly speaking, we cannot use \mathcal{I}_* as a criterion to be minimized—this quantity depends, as on a parameter, on the unknown to

²Namely, with $q = t\bar{q}$, $\bar{q} > 0$, one has $\mathbf{E}\{\|B\hat{x} - Bx_*\|_2^2\} = (1 + o(t))t^{-1}\mathcal{I}_*(\bar{q})$ as $t \rightarrow \infty$.

us true signal x_* . On the other hand, when replacing in the right hand side of (4) the unknown quantities $\rho_i^* := \exp\{-a_i^T x_*\}$ with their approximations ρ_i which are within factor c from ρ_i^* , that is $c^{-1}\rho_i^* \leq \rho_i \leq c\rho_i^*$, the resulting right hand side in (4) is within the same factor from the true one. Therefore, assuming that an approximate attenuation map ρ is available a priori, or that it can be estimated using observation $\bar{\omega}$ from a pilot run with, say, equal to each other “moderate” $\bar{q}_i = \bar{q}$, we may select q by minimizing over \mathcal{Q} the observable criterion

$$\mathcal{I}(q) = \text{Tr} \left(B \left[\sum_i q_i \rho_i a_i a_i^T \right]^{-1} B^T \right). \quad (5)$$

This is, essentially, the course of actions we propose.

2.5 Regularization

The problem of minimizing $\mathcal{I}(q)$ over $q \in \mathcal{Q}$ is convex and as such can, theoretically, be solved to whatever high accuracy in a computationally efficient manner. At the same time, numerical experimentation shows that this problem may happen to be ill-conditioned, resulting in difficulties when solving it numerically. To overcome, to some extent, these difficulties, we can replace minimizing over $q \in \mathcal{Q}$ the objective $\mathcal{I}(q)$ given by (5) with minimizing over the same domain the penalized objective

$$\mathcal{I}_\lambda(q) = \text{Tr} \left(B \left[\sum_i q_i \rho_i a_i a_i^T + \lambda I_n \right]^{-1} B^T \right) \quad (6)$$

where regularizing coefficient λ is nonnegative; a good value of this coefficient could be found experimentally. Thus, in the sequel we intend to optimize measurement design by solving convex optimization problem

$$\min_{q \in \mathcal{Q}} \left\{ \mathcal{I}_\lambda(q) := \text{Tr} \left(B \left[\sum_i q_i \rho_i a_i a_i^T + \lambda I_n \right]^{-1} B^T \right) \right\} \quad (7)$$

which can be solved by standard Convex Optimization algorithms. It turns out, however, that one can utilize problem’s structure to design a dedicated algorithm which, as our experiments show, is much faster than the “general purpose” algorithms. The following underlying observation is essentially well known:

Proposition 1. Let P be an $m \times n$ matrix of rank n , B be a $k \times n$ matrix, and q, ρ be positive m -dimensional vectors. Then, setting $W = W[q] := \text{Diag}\{q_i \rho_i, i \leq m\}$,

$$\mathcal{I}_\lambda(q) := \text{Tr} \left(B \left[\sum_i q_i \rho_i a_i a_i^T + \lambda I_n \right]^{-1} B^T \right)$$

$$= \begin{cases} \min_{G \in \mathbf{R}^{k \times m}} [\lambda^{-1} \|GA - B\|_F^2 + \text{Tr}(GW^{-1}G^T)], & \lambda > 0 \\ \min_{G \in \mathbf{R}^{k \times m}} [\text{Tr}(GW^{-1}G^T) : GA = B], & \lambda = 0 \end{cases} \quad (8a)$$

where $\|\cdot\|_F$ is the Frobenius norm

We provide the proof of Proposition 1 in Appendix A for the sake of completeness.

Alternating minimization. Proposition 1 suggests the *alternating minimization* algorithm for minimizing $\mathcal{I}_\lambda(q)$ over $q \in \mathcal{Q}$. Assume for the sake of definiteness that $\lambda > 0$ (modification for the case of $\lambda = 0$ is immediate). By (8a), the problem of interest (7) can be rewritten equivalently as

$$\min_{G \in \mathbf{R}^{k \times n}, q \in \mathcal{Q}} \Phi(G, q) := [\lambda^{-1} \|GA - B\|_F^2 + \text{Tr}(GW^{-1}(q)G^T)]$$

To solve the latter problem, we start with some positive $q^0 \in \mathcal{Q}$. At a step t of the algorithm, given positive $q^{t-1} \in \mathcal{Q}$,

- we minimize $\Phi(G, q^{t-1})$ over $G \in \mathbf{R}^{k \times m}$; this is an unconstrained minimization problem with strongly convex quadratic objective, and its solution G_t is given by explicit formula:

$$G_t = B[A^T W[q^{t-1}]A + \lambda I_n]^{-1} A^T W[q^{t-1}]; \quad (9)$$

- after G_t is computed, we specify q^t by minimizing $\Phi(G_t, q)$ over $q \in \mathcal{Q}$, which boils down to finding

$$q^t \in \underset{q \in \mathcal{Q}}{\text{Argmin}} \underbrace{\sum_{j=1}^m \frac{\|\text{Col}_j(G_t)\|_2^2}{q_j \rho_j}}_{=\text{Tr}(G_t W^{-1}[q] G_t^T)}.$$

When \mathcal{Q} is simple, the latter problem is simple as well. For instance, in the case of $\mathcal{Q} = \{q \in \mathbf{R}_+^m : c^T q \leq 1\}$ with $c > 0$, assuming that G_t has no zero columns (which can be ensured by an arbitrarily small perturbation of G_t), the solution is given by

$$[q^t]_j = \frac{r_j/c_j}{c^T r}, \quad r_j = \|\text{Col}_j[G_t]\|_2 \sqrt{c_j/\rho_j}, \quad 1 \leq j \leq m. \quad (10)$$

After G_t, q_t are computed, we pass to step $t + 1$.

3 Computational experiment

Here we report on a toy “proof of concept” numerical experiment on recovering $n = 32 \times 32$ -pixel Shepp-Logan type phantom with 68 projection angles spread uniformly over 360 degrees.

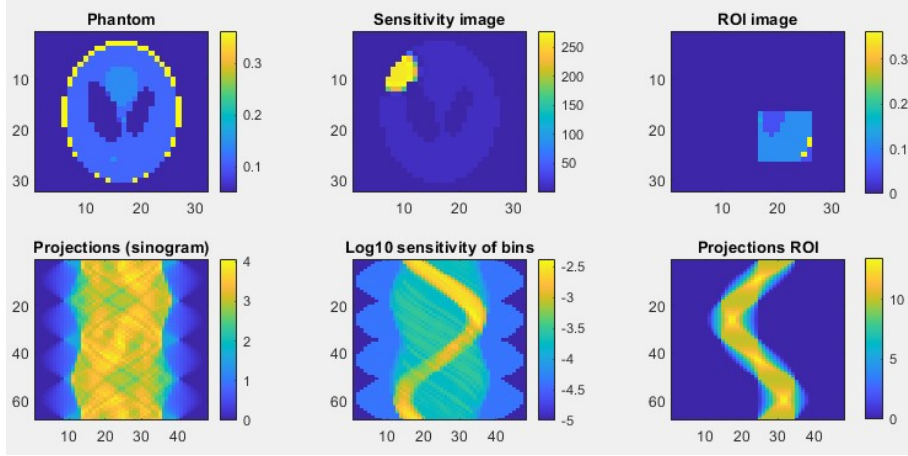


Figure 1: Top row: phantom, sensitivity image and region of interest (ROI). Bottom row: phantom sinogram, sensitivity of the bins and sinogram of the ROI.

3.1 Experimental setup

Unlike conventional tomography, where 180 degree angle span is sufficient, we consider 360 degree span to account for the fact that effective radiation dose is generally different when photons are sent along the same line from opposite directions due to different attenuation between the source and a particular body point. In our experiments, the number of bins is $m = 2828$; we utilize the baseline (uniform) radiation design $\bar{q}_i \equiv 2e5$ photons/bin. Figure 1, top row, shows the attenuation map, radiation sensitivity, and region of interest (ROI) which we aim to reconstruct. Bottom row shows the corresponding maps in the sinogram (projection) space. In particular, the middle picture shows radiation sensitivity in projection space, i.e. effective dose caused by a unit of radiation sent into each projection bin. One can see a bright curve strip of high sensitivity. As we will see later, our algorithm will reduce amount of radiation sent into this strip.

Building the field design vector q in the model presented in the previous section requires, along with the matrices A and B readily given by the geometry of bins and the ROI, the knowledge of vectors c and ρ with entries indexed by bins. The entries in c are proportional to our guess on effective dose from a single photon sent into the corresponding bin, and entries in ρ are estimations of the quantities $\exp\{-a_i^T x_*\}$. Both these vectors depend on the actual image x_* . “In real life” they may be either considered available a priori or should be obtained from a pilot recovery of x_* in which the radiation is a small fraction of R split, say, equally between m bins. In our “proof of concept” experiment where the goal is to understand potential of radiation design we use “ideal” values of ρ and c ; in particular, we set $\rho_i = \rho_i^* = \exp\{-a_i^T x_*\}$. To specify c

we act as follows: first, we utilize x_* and pixel sensitivities image s depicted in Figure 1 to compute the effective dose \bar{c}_i caused by a single photon sent through the bin i . Then, to get c , we scale \bar{c} to ensure that $c^T \bar{q} = 1$, where \bar{q} is the uniform (“baseline”) design such that the radiation in every bin is R/m .

3.2 Computations

Design optimization was carried out using alternating minimization (9)–(10) described in Section 2.5; 5–6 iterations of the process turned out to be sufficient to get high accuracy solution. An alternative, somehow more time consuming solution is provided by the first order algorithm—Mirror Descent with simplex setup, see [11, Lecture 5]. Maximum Likelihood estimate was computed utilizing Nesterov’s Fast Gradients [12] for minimizing smooth convex functions over the nonnegative orthant.

3.3 Numerical results

We present results of two experiments for the phantom image presented in Figure 1 and two values of the regularization parameter, $\lambda = 0$ and $\lambda = 1\text{e}3$. Figure 2 shows the obtained optimized radiation design in the penalized problem. The optimization results in significant reduction of radiation in the sensitive area and its increase in the ROI-related part of the sinogram. In each experi-

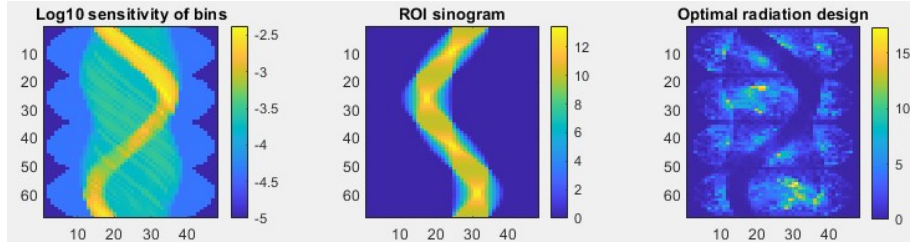


Figure 2: Radiation design for regularization $\lambda=1\text{e}3$ (right image.) For comparison, sensitivity and ROI sinograms are presented in the left and the middle plots.

ment we compute $N = 100$ recoveries utilizing baseline and optimized designs; in Figure 3 we present the histograms of the mean square error (MSE—squared recovery error per ROI pixel). Figure 4 shows typical recoveries of the ROI image in the case of $\lambda = 0$. One can observe a clear image quality improvement under the optimized design.

4 Concluding remarks

We present the first attempt to treat CT radiation design within a convex optimization framework. Unlike conventional design, it takes into account the

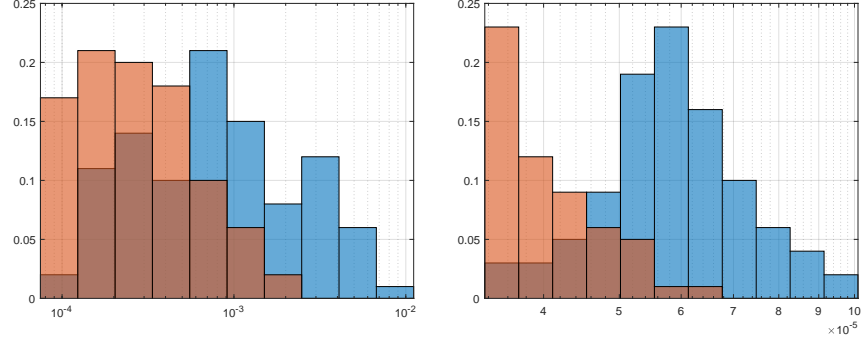


Figure 3: Distribution of the MSE in experiments with $\lambda = 0$ (left plot) and $\lambda = 1e3$ (right plot): blue histogram—baseline design, red histogram—optimized design.

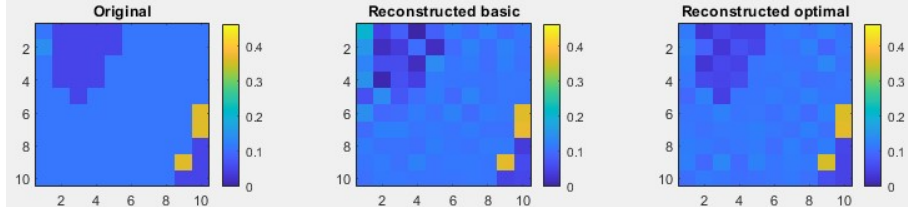


Figure 4: Original and reconstructed ROI (baseline and optimized designs), $\lambda = 0$.

radiation sensitivity map of the body, therefore minimizing the total effective dose.

Further challenges and opportunities

3D reconstruction In the 3D case the number of voxels scales as n^3 with single-dimension grid size, while the number of bins grows as n^4 . This gives much more degrees of freedom for the optimal design than in the 2D case. On the other hand, a faster algorithm is needed to implement radiation design in a reasonable time.

Our approach is especially attractive for use in radiation therapy rooms, where a preliminary radiation sensitivity map of a patient is readily available. It may be used e.g. with kilo-voltage cone-beam CT (kV-CBCT) systems integrated into the gantry of linear accelerators. [13, 14].

One more point to note: usually cone beam CT gantry moves with maximal axial speed so that each body point is exposed to x-ray only once for a given transaxial angle. It may be better to slow this movement down, allowing multiple axial x-ray angles for each transaxial angle. This would improve the reconstruction noise-to-dose ratio in CT systems in both cases, with and without

control of radiation pattern.

Radiation design under constraints In this work the design is optimized using an asymptotic maximum likelihood reconstruction model under unique effective dose constraint (2). One can easily impose extra convex constraints on the radiation vector q (e.g., total radiation dose, maximal dose per pixel, etc). Furthermore, the proposed design optimization framework can be adapted to account for the available a priori information about the body image when it is formulated in the form of convex constraints on the image space (cf., e.g., [15, Section 6.4.2]).

A Proof of Proposition 1

Given $m \times n$ matrix P of rank n and $\lambda > 0$, consider the optimization problem

$$\min_{H \in \mathbf{R}^{k \times m}} \{ \lambda^{-1} \|HP - B\|_F^2 + \|H\|_F^2 \}$$

The objective in this unconstrained minimization problem is a strongly convex quadratic function, so that optimal H is given the unique solution to the Fermat equation

$$\lambda^{-1} P[P^T H^T - B^T] + H^T = 0,$$

resulting in

$$H = B[\lambda^{-1}P][\lambda^{-1}PP^T + I_m]^{-1} = B[P^T P + \lambda I_n]^{-1}P^T,$$

where the second equality is due to Sherman-Morrison formula. Direct computation shows that for this H one has

$$\lambda^{-1} \|HP - B\|_F^2 + \|H\|_F^2 = \text{Tr}(B[P^T P + \lambda I_n]^{-1}B^T).$$

Setting $P = W^{1/2}A$ and substituting the optimization variable H with $GW^{-1/2}$, we arrive at (8a). Passing in the latter relation to limit as $\lambda \rightarrow +0$ and taking into account that A is of rank n , we arrive at (8b). \square

References

- [1] G. J. Gang, J. H. Siewerdsen, and J. W. Stayman, “Task-driven optimization of fluence field and regularization for model-based iterative reconstruction in computed tomography,” *IEEE transactions on medical imaging*, vol. 36, no. 12, pp. 2424–2435, 2017.
- [2] T. P. Szczykutowicz and C. A. Mistretta, “Design of a digital beam attenuation system for computed tomography: Part i. system design and simulation framework,” *Medical physics*, vol. 40, no. 2, p. 021905, 2013.

- [3] S. S. Hsieh and N. J. Pelc, “The feasibility of a piecewise-linear dynamic bowtie filter,” *Medical physics*, vol. 40, no. 3, p. 031910, 2013.
- [4] F. Liu, G. Wang, W. Cong, S. S. Hsieh, and N. J. Pelc, “Dynamic bowtie for fan-beam ct,” *Journal of X-ray Science and Technology*, vol. 21, no. 4, pp. 579–590, 2013.
- [5] W. Peppler, B. Kudva, J. Dobbins III, C. Lee, M. Van Lysel, B. Hasegawa, and C. Mistretta, “Digitally controlled beam attenuator,” in *Application of Optical Instrumentation in Medicine X*, vol. 347, pp. 106–111, SPIE, 1982.
- [6] T. P. Szczykutowicz and J. Hermus, “Fluid dynamic bowtie attenuators,” in *Medical Imaging 2015: Physics of Medical Imaging*, vol. 9412, pp. 219–225, SPIE, 2015.
- [7] P. Shunhavanich, S. S. Hsieh, and N. J. Pelc, “Fluid-filled dynamic bowtie filter: a feasibility study,” in *Medical Imaging 2015: Physics of Medical Imaging*, vol. 9412, pp. 399–406, SPIE, 2015.
- [8] F. Liu, Q. Yang, W. Cong, and G. Wang, “Dynamic bowtie filter for cone-beam/multi-slice ct,” *PloS one*, vol. 9, no. 7, p. e103054, 2014.
- [9] J. W. Stayman, A. Mathews, W. Zbijewski, G. Gang, J. Siewersen, S. Kawamoto, I. Blevis, and R. Levinson, “Fluence-field modulated x-ray ct using multiple aperture devices,” in *Medical Imaging 2016: Physics of Medical Imaging*, vol. 9783, pp. 232–237, SPIE, 2016.
- [10] A. Mathews, G. Gang, R. Levinson, W. Zbijewski, S. Kawamoto, J. Siewersen, and J. Stayman, “Experimental evaluation of dual multiple aperture devices for fluence field modulated x-ray computed tomography,” in *Medical Imaging 2017: Physics of Medical Imaging*, vol. 10132, pp. 690–695, SPIE, 2017.
- [11] A. Ben-Tal and A. Nemirovski, “Lectures on modern convex optimization (2020),” *SIAM, Philadelphia, PA. Google Scholar Google Scholar Digital Library Digital Library*, 2021.
- [12] Y. Nesterov, *Lectures on convex optimization*, vol. 137. Springer, 2018.
- [13] K. Srinivasan, M. Mohammadi, and J. Shepherd, “Applications of linac-mounted kilovoltage cone-beam computed tomography in modern radiation therapy: A review,” *Polish journal of radiology*, vol. 79, p. 181, 2014.
- [14] J. Wang, T. Li, Z. Liang, and L. Xing, “Dose reduction for kilovoltage cone-beam computed tomography in radiation therapy,” *Physics in Medicine & Biology*, vol. 53, no. 11, p. 2897, 2008.
- [15] A. Juditsky and A. Nemirovski, *Statistical Inference via Convex Optimization*. Princeton University Press, 2020.